Nano Today 25 (2019) 13–26

Contents lists available at ScienceDirect

Nano Today

journal homepage: www.elsevier.com/locate/nanotoday

Review

Liquid bridge induced assembly (LBIA) strategy: Controllable one-dimensional patterning from small molecules to macromolecules and nanomaterials

Chunze Yan[a], Bin Su[a,*], Yusheng Shi[a], Lei Jiang[b,*]

[a] State Key Laboratory of Material Processing and Die & Mould Technology, School of Materials Science and Engineering, Huazhong University of Science and Technology, Wuhan 430074, PR China
[b] Laboratory of Bioinspired Smart Interfacial Science, Technical Institute of Physics and Chemistry, Chinese Academy of Sciences, Beijing 100190, PR China

ARTICLE INFO

Article history:
Received 11 September 2018
Received in revised form 19 January 2019
Accepted 26 February 2019
Available online 14 March 2019

Keywords:
Wettability
Liquid bridge
One-dimension (1D)
Assembly
Patterning

ABSTRACT

One-dimensional (1D) assemblies/structures of functional nanomaterials are able to directionally transport electrons, excitons, photons or phonons, and gather scientists' attentions due to their potential applications in diverse fields. However, overlapped, crosslinking or other randomly dispersed 1D assemblies/structures appear after the solution process, which greatly restricts their practical device applications. In this Review, recent progresses in precisely positioning 1D patterning, from small molecules to macromolecules and nanomaterials, through a liquid bridge induced assembly (LBIA) strategy have been summarized. The keys to tailor the location, as well as the structure of as-prepared 1D assembles are discussed. Then, a rule for the selection of materials in the LBIA strategy has been proposed. Finally, some representative device applications of 1D assembles are demonstrated. It is believed that ordered 1D assemblies/structures of functional nanomaterials through the LBIA process will offer new opportunities that might favor different application fields.

Contents

Introduction

One-dimensional (1D) assemblies/structures of functional nanomaterials can directionally transport electrons, excitons, pho-

* Corresponding authors.
E-mail addresses: subin@hust.edu.cn (B. Su), jianglei@iccas.ac.cn (L. Jiang).

https://doi.org/10.1016/j.nantod.2019.02.010
1748-0132/

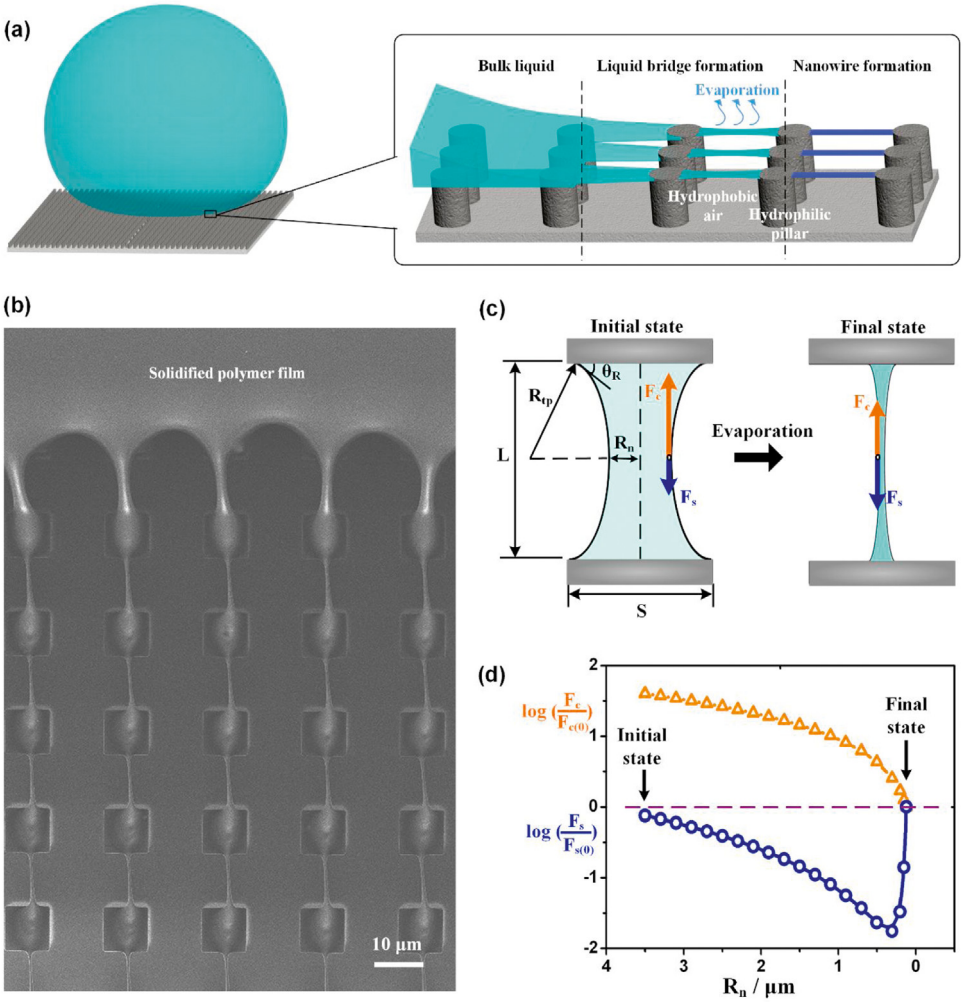

Fig. 1. Superhydrophobic pillar-structured substrates lead to regular liquid bridge arrays. (a) Schematic illustration and (b) a SEM image of the formation process of aligned nanowires during the regular liquid rupture upon a superhydrophobic pillar-structured substrate. (c) Schematic illustration of F_c and F_s inside one liquid bridge. (d) The dependence of F_c and F_s on the radius of the liquid bridge neck (R_n). With the evaporation of water, such two forces are equal to each other. Reprinted from Ref. [55] with permission from Wiley-VCH Verlag GmbH & Co.

tons or phonons [1–4], and exhibit considerable applications in high-density microcircuits, waveguiding, field-effect transistors, highly sensitive sensors, logic computations and others [5–27]. Owing to its low-cost, room-temperature and easy-to-large-scale advantages, solution-processed strategies are commonly used in the fabrication of 1D assembled materials [28–30]. Traditional solution processes, such as drop-casting, spin-coating or inkjet printing, are difficult to control their dewetting behaviors. As a result, randomly dispersive 1D assemblies/structures of functional materials appear, indicating limited application due to their overlapped/crosslinking status. Therefore, the challenge of manipulating the dewetting behavior in the solution processes is prerequisite [31–49].

Wettability control is a powerful tool to govern the dewetting of liquids upon the solid surfaces [50,51]. Lyophilic solid surfaces prefer to spread the liquid while lyophobic counterparts commonly repel the liquid. At the molecular level, the top atomic/molecular layer of the lyophilic areas attract the liquid molecules while those in the lyophobic regions will repel the liquid molecules to other places. Accordingly, the dewetting of liquid can move from the lyophobic (low-surface-free-energy) area towards the lyophilic (high-surface-free-energy) region, allowing for the liquid to climb uphill [52], directional condense [53], and on-demand transport in the microfluidics [54]. Besides the macroscopic motions, in recent decades, the control of wettability has been recognized as an effective route to dominate the liquid dewetting at the microscale [55]. When introducing regular lyophilic dots/stripes onto a lyophobic surface, highly ordered liquid bridges with several micrometers can appear. At the beginning, each liquid bridge was several micrometers in width and tens of micrometers in length. Due to the evaporation of volatile solvent, the width of each liquid bridge will shrink gradually. In this case, each liquid bridge can serve as a linear confined spacing to restrict the assembly of inside guests, leading to ordered 1D arrangement of functional materials. Most importantly, the patterning, including location, orientation and density, of microscale liquid bridges is tunable by a careful design of lyophilic/lyophobic domains, resulting in precisely positioning 1D assemblies. This wettability-controlled liquid bridge induced assembly strategy can circumvent the positioning challenge of 1D assemblies in the solution process.

In this Review, recent progress in precisely positioning 1D patterning, from small molecules to macromolecules and nanomaterials, through a liquid bridge induced assembly (LBIA) strategy [7,55–79] will be briefly reviewed. First part introduces basic theories on the generation of wettability dominated liquid bridge arrays. Second section mainly discusses diverse methods to tailor the location, as well as the structure of as-prepared 1D assembles. The third

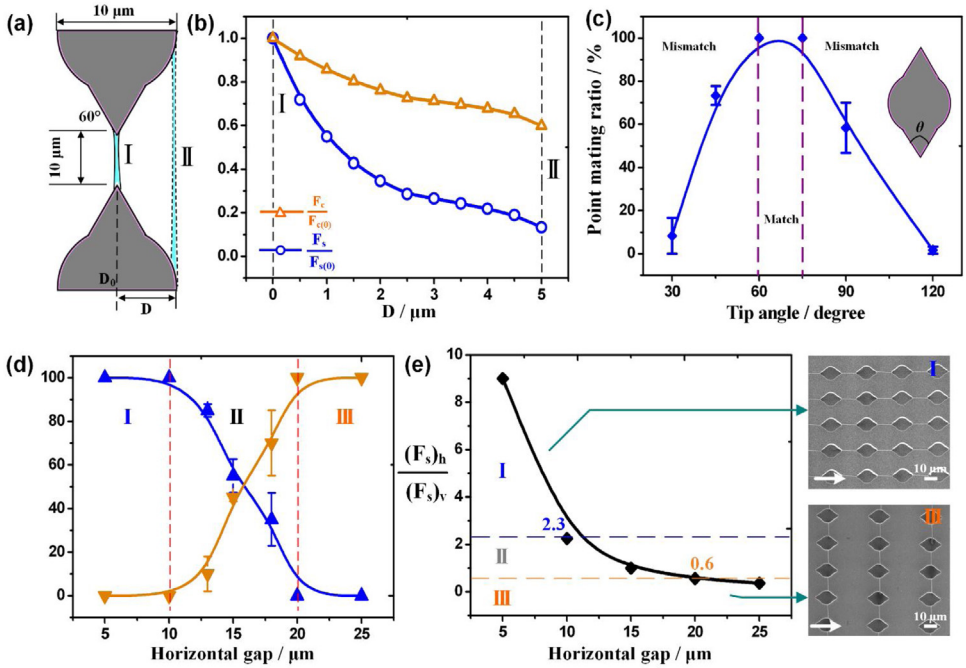

Fig. 2. Tip-induced effectand nearest bridging rulein the liquid bridge induced assembly (LBIA) strategy. (a) Schematic illustration of 1D assembly located between a pair of tip-to-tip shaped micropillars. (b) Dependence of F_c and F_s on the position of tip-shaped micropillars. (c) Dependence of position mating ratio on the tip angle of micropillars. (d) Variation of horizontal (blue) and vertical (orange) nanowire formation ratio with the tip distance. (e) Variation of the ratio of F_s in the horizontal and vertical directions with tip distance. Right images are representative SEM images of nanowire patterns. Reprinted from Ref. [55] with permission from Wiley-VCH Verlag GmbH & Co., Ref. [77] with permission from American Chemical Society.

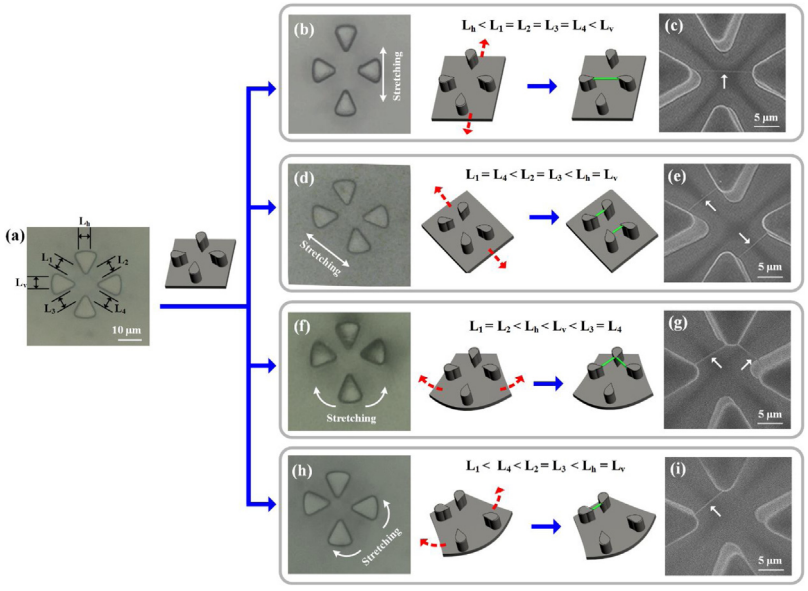

Fig. 3. Dynamic strategies to tailor the positioning of as-prepared 1D assemblies in the LBIA process. (a) Soft and stretchable pillar-structured PDMS substrate can change the pillar gaps by external forces, yielding different wire patterns. (b,c) one horizontal nanowire, (d,e) parallel nanowires, (f,g) herringbone-shaped nanowires and (h,i) one 45° nanowire generated on the same substrate by stretching in different directions. Reprinted from Ref. [77] with permission from American Chemical Society.

part shows the species of functional materials that can be assembled through the LBIA strategy, and propose a rule to guide the selection of materials. Both organic and inorganic guests can be assembled in the LBIA process. In the fourth part, representative applications of LBIA dominated 1D assembles, such as fluorescent sensors, waveguiding, microcircuits, field effect transistors, pressure sensors and magnetic detectors, are demonstrated. Finally, a brief conclusion and outlook will be provided.

Liquid bridge induced assembly (LBIA) mechanism

When a volatile liquid is dropped onto a solid surface, its three phase contact line (TCL) will shrink towards its geometric center driven by the evaporation. The dewetting process of the liquid upon a homogenous solid surface is continuous, however, will be interrupted by wettability-heterogeneous domains (Fig. 1a). Superhydrophobic (water contact angles > 150°) pillar-structured substrates are the most used strategy to prepare

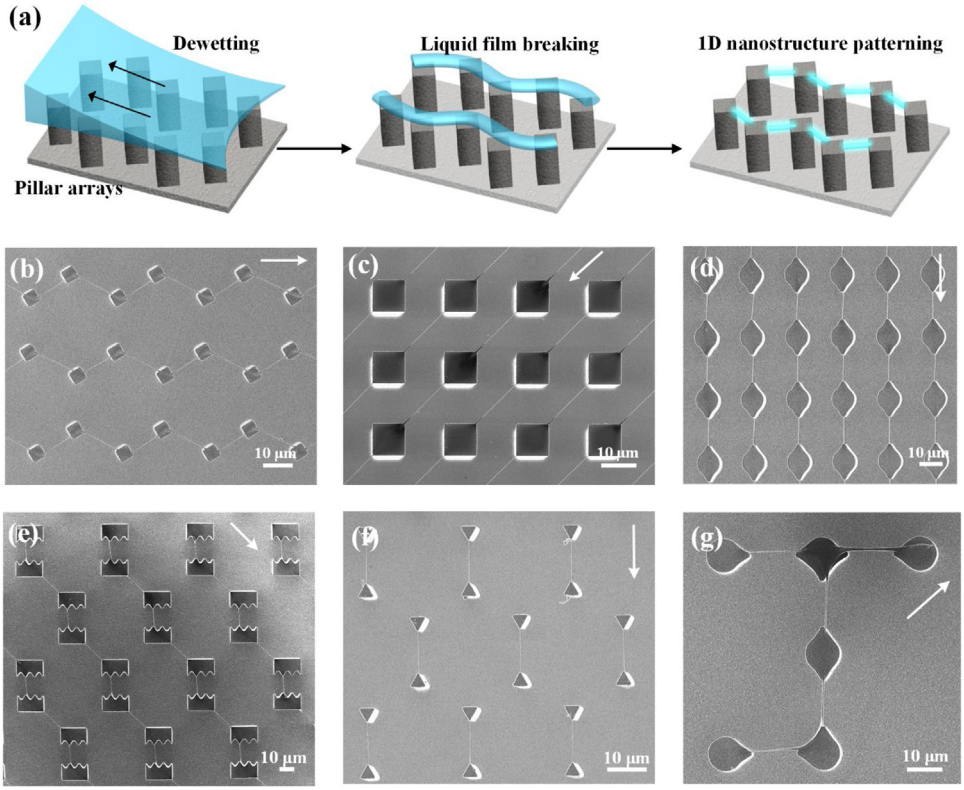

Fig. 4. On-demand positioning of as-prepared 1D assemblies by pre-designed pillar patterns. (a) Schematic illustrations of the breaking of liquid films on a pillar-structured substrate, allowing the formation of zigzag type wire arrays. SEM images of precisely positioning wire patterns on (b,c) square, (d) spindle, (e) toothing, (f) triangle and (g) J̌šhaped micropillars. Reprinted from Ref. [55] with permission from Wiley-VCH Verlag GmbH & Co.

wettability-heterogeneous solid surfaces. No matter consisting of soft polydimethylsiloxane (PDMS) rubber [80–87] or rigid silicon crystalline [7,55–79], the basic mechanism of pillar-structured substrates is based on the hydrophilic pillar tops collaborated with hydrophobic air pockets trapped in the pillar gaps (inset image of Fig. 1a). Generally, the surfaces of micropillars are modified by a thin-layer of low-surface-free-energy molecules to resist the permeation of liquid. Even the pillar tops are liquid-resistant, they serve as the hydrophilic domains in the LBIA strategy since the air pockets trapped in the pillar gaps are more hydrophobic. When the TCL of liquids begin to move upon a pillar-structured substrate, each pillar top works as the hydrophilic domain to firmly pin the liquid. At the meanwhile, the air pockets trapped in the pillar gaps can serve as the hydrophobic domains to rupture the liquid films. Therefore, microscale liquid bridge arrays appear connecting neighbouring micropillars (Fig. 1b).

Two competitive forces exist inside each microscale liquid bridge. One is capillary force, F_c, which is dominated by the surface tension and capillary pressure at the fluid/solid interface, and the other is structural cohesive force, F_s, which is the mechanical strength of liquid bridges (Fig. 1c). With the evaporation of water, the narrowing of liquid bridges leads to decreased F_c and increased F_s (Fig. 1d). Finally, such two forces were comparable with each other ($F_{c(0)}$ is equal to $F_{s(0)}$). The liquid bridges connect neighbouring lyophilic domains, indicating the dewetting process of the liquid bridges will proceed in the width direction, rather than along the length direction. With the narrowing of liquid bridges, their inside guests will be forced to pack in one direction, resulting in 1D assemblies of functional materials, known as the LBIA mechanism.

The location of liquid bridges highly depends on the geometry of micropillars [55]. A ẗip-induced effectc̈ommonly exists on spindle shaped micropillars (Fig. 2a). By analyzing the forces locating in different positions, it is easy to find that the ratio of F_s/F_c increases more than 4 times from Position II to Position I (Fig. 2b). As a result, liquid bridges between the tips exhibit stronger structural force, indicating a more stable state for the generation of 1D assembly. The tip angles of spindle shaped micropillars also affect the positioning. 60°-75° is optimized values for precise positioning of resulted 1D assemblies (Fig. 2c). Besides tip angles, the distance between the tips dramatically dominated the patterning, as well as positioning, of 1D assemblies, named as n̈earest bridging rule[̈77]. By fixing the vertical pillar gap at 10 μm while changing the horizontal distance between the tips from 5 to 25 μm, it can be clearly found that horizontal nanowires were gradually reduced, while vertical counterparts increased dramatically (Fig. 2d). Fig. 2e shows the relationship between $(F_s)_h/(F_s)_v$ and tip distance (L). Larger tip distance indicates increased structural force (F_s) that will break the resulted 1D assemblies. Therefore, horizontal nanowire arrays will change to vertical ones following the increase of the tip distance. In summary, the 1D assemblies from the LBIA process prefer to bridge nearest micropillars.

Controllable patterning and structures of 1D assemblies

Tunable patterns

The patterning, including location, orientation and density, of 1D assemblies in the LBIA strategy highly depends on the generation of liquid bridges. By understanding above ẗip-induced effectänd n̈earest bridging rulëin the LBIA process, a dynamic strategy was proposed to control the positioning of nanowires based on a stretchable pillar-structured PDMS substrate [77]. Rhombus-patterned micropillars on the soft film were molded from the rigid

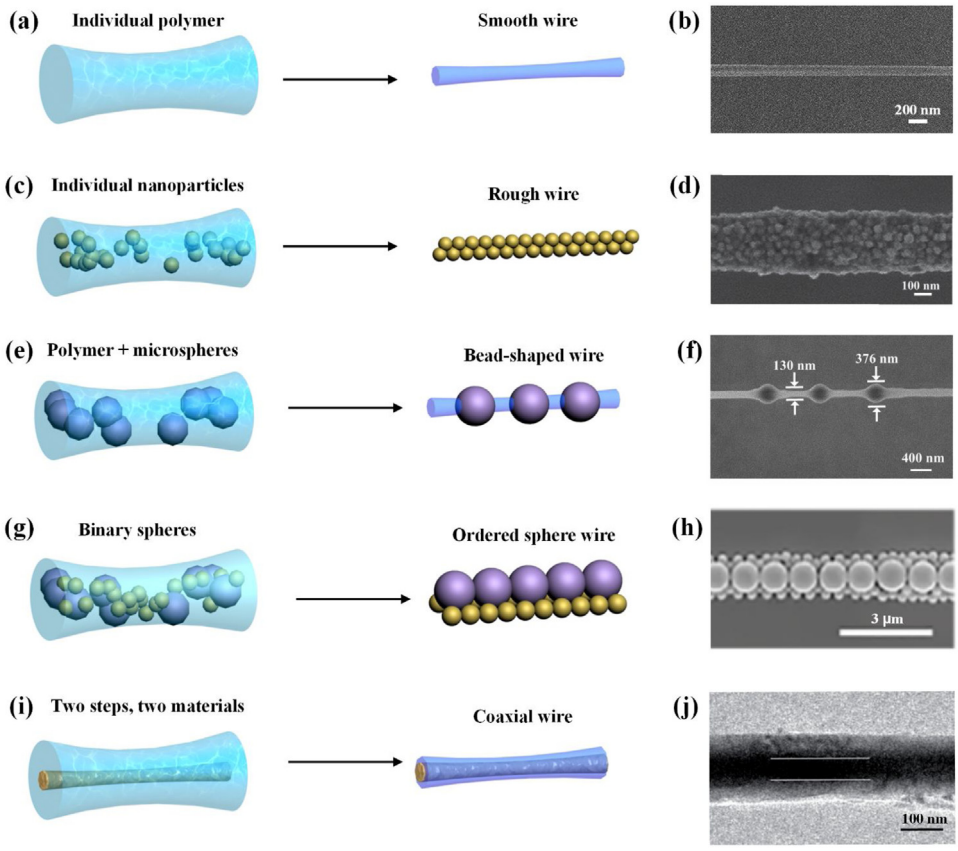

Fig. 5. Methods to tune the structures of as-prepared 1D architectures in the LBIA process. Schematic illustrations of (a) smooth, (c) rough, (e) bead-shaped, (g) 1D binary superstructural and (i) coaxial structures wires through the LBIA processes. (b), (d), (f), (h) are corresponding SEM images of (a), (c), (e), (g), respectively. (j) is corresponding TEM image of (i). Reprinted from Ref. [55,58,75] with permission from Wiley-VCH Verlag GmbH & Co., Ref. [61]. with permission from Royal Society of Chemistry, Ref. [88] with permission from American Chemical Society.

silicon template (Fig. 3) with equal horizontal and vertical pillar gaps. When the soft substrate was stretched in the vertical direction, the distance of vertical pillar gap was larger than that in the horizontal direction. In this case, only one nanowire was fabricated, whereas none of wire existed to bridge the vertical micropillars. On the other hand, if the soft substrate was stretched in 45° or just one side, the distance of pillar gap will be changed accordingly, leading to diverse wire patterns.

Besides soft micropillars, the geometric shapes, as well as the locations of hydrophilic domains, were tailored to effectively govern the patterning of 1D assemblies. Taking the polyvinyl alcohol (PVA) nanowire patterning as an example, a zigzag type pattern appeared by carefully designing the location of micropillars (Fig. 4a,b) [55,58]. If the dewetting direction of liquid was 45° inclined towards square-shaped micropillars, the nanowires could precisely locate at the corners of each micropillar due to the shortest distance between the neighbouring hydrophilic domains (Fig. 4c). This discovery has been further proved by utilizing a spindle-shaped micropillars (Fig. 4d). The nanowires would appear just to bridge the tips of neighbouring micropillars, indicating a precise strategy to control the positioning of 1D assemblies. By fabricating diverse pillar shapes and locating them in the pre-designed position, the nanowires could be a zigzag shape (Fig. 4e), discontinuous type (Fig. 4f) and an alphabet J̈p̈atterning (Fig. 4g).

Tunable structures

Generally, the shape of 1D assemblies through the LBIA strategy was smooth (Fig. 5a,b) [55,59,64,68,77] or rough (Fig. 5c,d) [58,61,67] due to homogenous narrowing of liquid bridges containing individual building blocks. However, the result might be different when mixing two-component building blocks, such as ẗhardp̈olystyrene (PS) microspheres and s̈oftP̈VA molecules, into the liquid bridges (Fig. 5e) [75]. With the narrowing of the liquid bridges, the PS microspheres and PVA molecules were forced to align. Because the size of firm PS microspheres (hundreds of nanometers) was larger than the width of PVA wire (tens of nanometers), bead-shaped wires were generated accordingly (Fig. 5f). The PS microspheres served as the bead parts while the PVA wires bridged the neighbouring PS beads, leading to artificially spindle silks at the microscale. Besides bead-shaped nanowires, 1D binary superstructures, consisting of PS spheres within different sizes, have been reported by Song et al [88]. In this study, large PS spheres were mixed with small PS ones (the diameter of two species was around 6–8, see Fig. 5g). After undergoing the LBIA process, small PS spheres preferred to stay at the bottom sides of the larger counterparts, yielding 1D binary superstructures (Fig. 5h).

Coaxial 1D microstructure, consisting of heterogeneous materials in its core and sheath parts, can be fabricated by a two-step LBIA process [61]. First, highly oriented calcein wire arrays were fabricated, and covered by a thin layer of fluoride molecules to prevent the damage from the second LBIA process. Then, a neil-red-rich liquid was used to form the outside sheath parts, yielding calcein@nile-red coaxial wire arrays (Fig. 5i). From the transmission electron microscope (TEM) image shown in Fig. 5j, a clear coaxial structure can be found. Importantly, these two functional materials, selected in the core and sheath parts, can generate fluorescence resonance energy transfer (FRET) due to their overlapped energy bands. In this case, the coaxial wire arrays can serve as the chemical sensors to respond diverse metallic/organic compounds. Further-

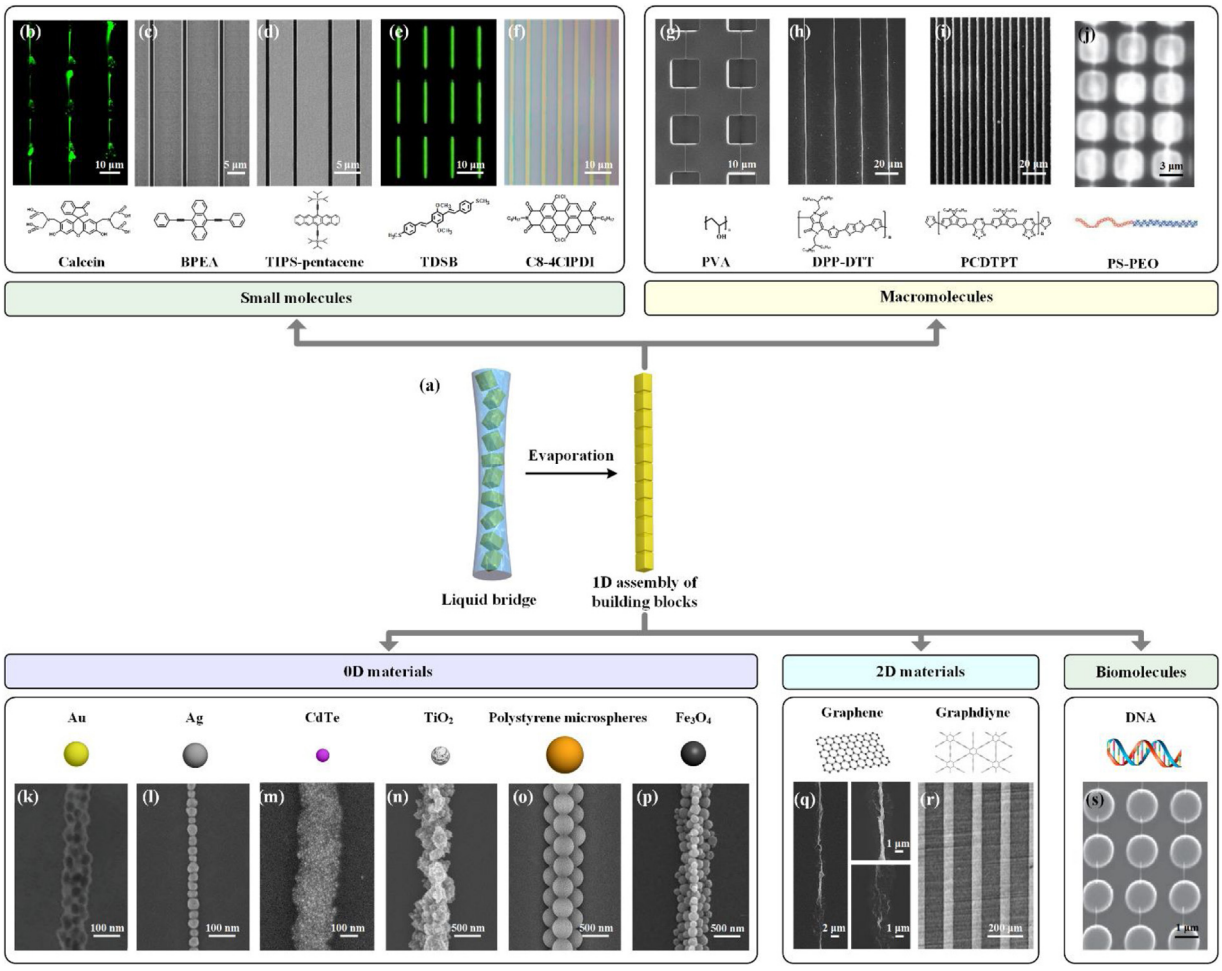

Fig. 6. Diverse material species can be assembled into 1D architectures through the LBIA strategy. (a) Schematic illustration of a LBIA process. Small molecules, including (b) calcein, (c) 9,10- bis(phenylethynyl)anthracene (BPEA), (d) 6,13-bis(triisopropylsilylethynyl) pentacene (TIPS-pentacene), (e) 1,4-dimethoxy-2,5-di[4-(methylthio)styryl]benzene (TDSB) and (f) alkyl substituted core-tetrachlorinated perylene diimides (R-8ClPDIs), macromolecules, such as (g) poly(vinyl alcohol) (PVA), (h) dithienylthieno[3,2-b] thiophene-*N*-alkyl diketopyrrolo-pyrrole (DTT-DPP), (i) poly [4-(4,4-dihexadecyl-4H-cyclopenta[1,2-*b*:5,4-*b*']dithiophen-2-yl)-alt- [1,2,5] [3,4-c]pyridine] (PCDTPT) and (j) polystyrene-poly(ethylene oxide) diblock copolymer (PS-PEO), 0D materials, including (k) gold, (l) silver, (m) cadmium telluride, (n) titaninm dioxide, (p) ferriferrous oxide particles and (o) polystyrene (PS) microspheres, and 2D materials, such as (q) graphene or (r) graphdiyne, and biomolecules, such as (s) deoxyribonucleic acid (DNA) double helix, can all be assembled into 1D architectures through the LBIA strategy. Reprinted from Ref. [55,64–68,70,74,76,86,87,97,98] with permission from Wiley-VCH Verlag GmbH & Co., Ref. [60] with permission from Nature Publishing Group, Ref. [79] with permission from American Chemical Society.

more, another coaxial 1D structure consisting of rigid inorganic core and soft organic sheath was demonstrated [58]. 1D assemblies of silver NPs in the core part transported electrons while PS was used to prevent the sulfuration from the atmosphere. Compared with bare silver NP wires, the silver-NP@PS coaxial 1D structures showed a stable electrical performance even after stored in one month. Boukany's group reported a one-step strategy to build coaxial 1D structures based on the self-organization of polystyrenepolyethylene oxide block- copolymer (PS-b-PEO) micelles [89]. During the LBIA process, rigid PS molecular segments self-assembled into the core part, leaving the soft PEO segments as the sheaths.

1D assemblies of diverse material species

The liquid bridges in the LBIA strategy connect neighbouring lyophilic domains, indicating the dewetting process of the liquid bridges will proceed in the width direction, rather than along the length direction. With the narrowing of liquid bridges, their inside guests will be forced to pack in one direction, resulting in 1D assemblies of functional materials (Fig. 6a). Then, one question has been raised: what kinds of materials can be assembled in the LBIA strategy? To address this point, three criteria have been proposed to guide the selection of materials: (1) The liquid should be volatile. The evaporation of liquid is the driving force of dewetting, and the source of the liquid bridge generation. (2) The functional materials should homogenously disperse in the liquid no matter they are dissolved or in a suspended state. (3) The interaction among the functional materials should be large enough to hold their mechanical strength after the dewetting process.

Small molecules

Taking the calcein molecules as an example, we exhibit their 1D assemblies through the LBIA strategy. Calcein is a kind of small molecules that owns four carboxyl groups at both its sides (Fig. 6b). The calcein molecules can completely dissolve (criteria (2)) in the water (criteria (1)), and formed considerable hydrogen bonds (criteria (3)) to link themselves after dewetting. By placing a calcein-rich drop upon the pillar-structured substrate, highly oriented calcein microwire arrays could be fabricated [68], which showed green fluorescence when exposed to a UV excitation. The interaction among the molecules is the key to build firm 1D assemblies. Other two molecules (fluorescein and 5-carboxyfluorescein) whose structures own the same middle part but fewer carboxyl

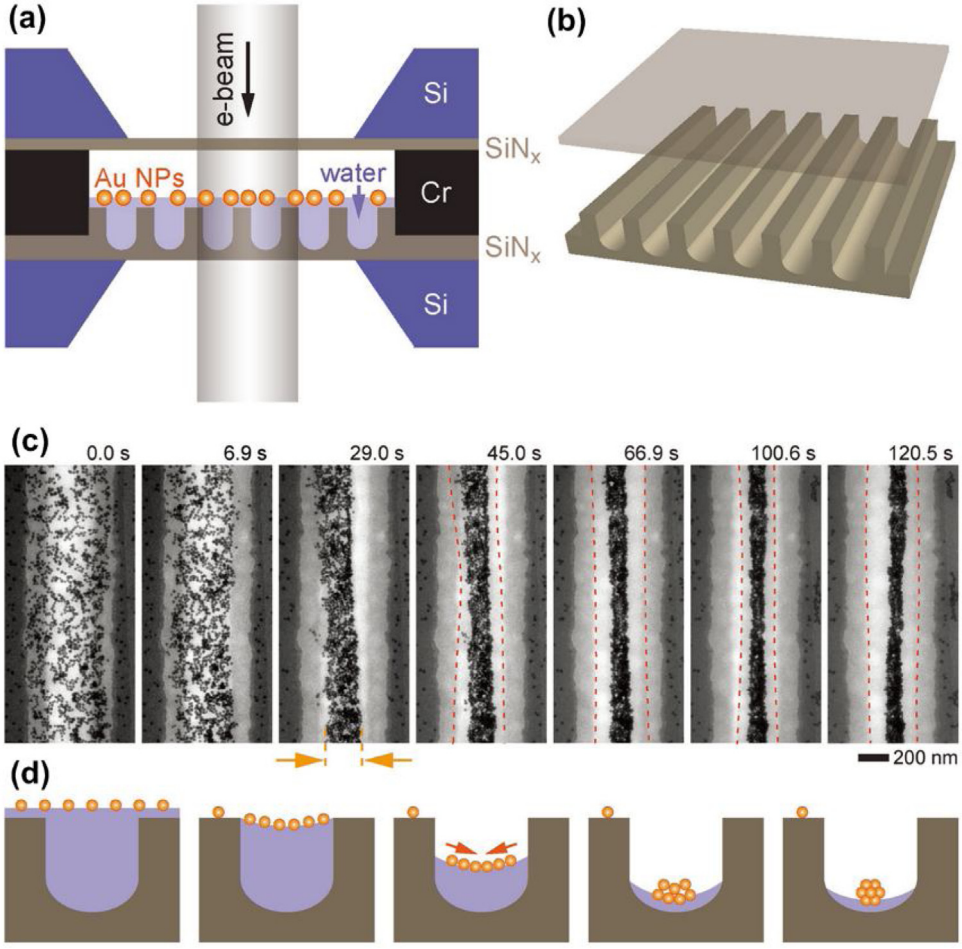

Fig. 7. In-situ TEM observation of the formation of 1D assembly of NPs driven by shrinking space inside evaporated water stripes. (a,b) Schematic illustrations of the experimental setup. A solution of hydrophobic GNPs was encapsulated between a nanochannel-structured silicon nitride (SiN_x) and a top flat one. (c) In situ TEM image series showing the process of NP 1D assembly following the evaporation of water. (d) Schematic illustrations of the cross-sectional parts according to (c), respectively. Reprinted from Ref. [96] with permission from Wiley-VCH Verlag GmbH & Co.

groups at their sides have been also tried through the LBIA process. However, reduced carboxyl groups greatly suppressed the generation of hydrogen bonds between neighbouring molecules, yielding bare small molecular wire.

π–π stacking interactions, as well as hydrogen bonds, are two major molecular non-covalent interactions to assemble organic 1D architectures. In 2015, Jiang and Su et al. utilized a top-lyophobic & side-lyophilic grooved substrate to guide the 1D assemblies of 9,10- bis(phenylethynyl)anthracene (BPEA) small molecules (Fig. 6c) [60]. Owing to its planar and benzene-ring-rich molecular structure, the BPEA molecules firstly π–π stacked on the silicon substrate with (100) plane, then grew along the [010] direction, resulting in single-crystalline small molecular wires. Similar mechanism has been used to guide the generation of single-crystalline 6,13-bis(triisopropylsilylethynyl) pentacene (TIPS- pentacene, see Fig. 6d) [65], 1,4-dimethoxy-2,5-di[4-(methylthio)styryl]benzene (TDSB, see Fig. 6e) [74] and alkyl substituted core-tetrachlorinated perylene diimides (R-8ClPDIs, see Fig. 6f) microwire/belt arrays [79].

Macromolecules

Poly(vinyl alcohol) (PVA) is a kind of water-soluble polymer. When a PVA-rich drop was slipped upon the pillar-structured substrate, highly ordered PVA nanowire arrays were achieved (Fig. 6g) [55]. Free-standing PVA nanowires could be fabricated within 10 s. By using the similar approach, flexible deoxyribonucleic acid (DNA) double helix biomolecular wires can be arranged towards one direction with a width of tens of nanometers (Fig. 6s) [80–86,89–93]. Since the LBIA strategy provided linear confined spacing with a high length-width ratio, flexible DNA chains would undergo a coil-stretch transition [94,95]. Lee and Boukany et al. reported this visible DNA coil-stretch transition by using a micropatterned substrate [80,94,95]. Following the dewetting of the droplet, DNA chains insides liquid bridges would be stretched bridging neigoubouring micropillars. Besides flexible macromoleculs, rigid planar macromolecules, such as dithienylthieno[3,2-b] thiophene-*N*-alkyl diketopyrrolo-pyrrole (DTT-DPP, see Fig. 6h) [64] or poly [4-(4,4-dihexadecyl-4H-cyclopenta[1,2-*b*:5,4-*b*']dithiophen-2-yl)-alt- [1,2,5] [3,4-c]pyridine] (PCDTPT, see Fig. 6i) [76], and polystyrene-poly(ethylene oxide) diblock copolymer (PS-PEO) (Fig. 6j) [87], can also be assembled towards one direction through the LBIA strategy. Since most functional polymers are insoluble in water, benzene derivative liquids were used in these studies.

0D nanomaterials

Above-mentioned small molecules [60,65,68,74,79] or polymers [55,64,76,80–87,89–93] are completely dissolved in the

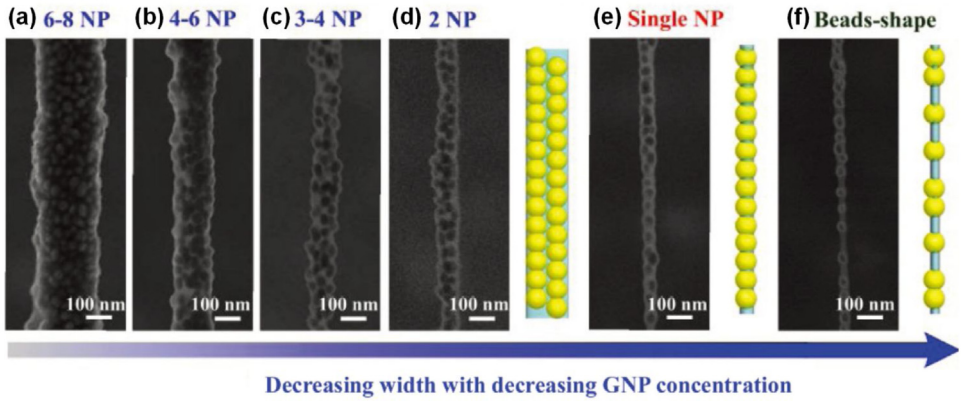

Fig. 8. The LBIA strategy can tune the width of NP 1D assembly. TEM images of GNP 1D assemblies with tunable widths from (a) 6–8, (b) 4–6, (c) 3–4, (d) 2 to (e) single particle size by decreasing the GNP/PVA ratio. Reprinted from Ref. [67] with permission from Wiley-VCH Verlag GmbH & Co.

liquid. In contrast, most 0D nanomaterials, capped by diverse ligands to prevent their aggregation, just stably suspend in the liquid during the LBIA process. At the beginning, 0D nanomaterials could randomly move inside the liquid due to the Brownian motions. However, their free motions were gradually restricted along with the narrowing of liquid bridges, yielding regular 1D assemblies. In these cases, the interaction among the particles is mostly governed by the van de Waals force, rather than covalent/non-covalent chemical bonds.

Very recently, this LBIA dominated 1D assembly of NPs was directly observed by Mirsaidov et al. through an in-situ liquid-cell transmission electron microscopy (LC-TEM) [96]. The experimental platform was schematically shown in Fig. 7a. Golden nanoparticles (GNPs) solution was sandwiched between two translucent SiNx films. In particular, the bottom SiNx film was fabricated with microchannel structure while the top one was flat (Fig. 7b). Based on this special cell design, the stepwise self-assembly dynamics of hydrophobic GNPs into 1D assembly can be directly observed (Fig. 7c). First, a meniscus of water stripe formed between neighbouring nanochannel walls. With the slow evaporation of water, GNPs gradually accumulated in the middle part of the water stripe. Owing to the strong van der Waals attraction between the ligands outside particle surfaces, dispersive nanoparticles were closely compact along the water stripe direction, yielding 1D assembly of GNPs in the centers of the nanochannels (Fig. 7d).

Since the occupation probability of each particle is the same in the LBIA process, high concentrated particle suspension leads to wider 1D assemblies, while dilute liquid can result in narrow, even single particle in width, linear architectures. Taking the GNPs as an example [67], the GNPs with diameter of ~45 nm were mixed with PVA and assembled upon pillar-structured substrates (Fig. 6k). Ordered zigzag-type GNP assemblies could be prepared, whose widths were tunable ranging from 6 to 8 GNPs to single GNP, and even bead-shaped nanowires (Fig. 8). Within ultra-low GNP concentration in the polymeric solution, sparse GNPs were connected by thin PVA wires after undergoing the LBIA [78] process (see Fig. 8f). Soon after that, grooved substrates were used to guide the assembly of silver NPs (SNPs) [66]. 1D architecture with single particle in width was achieved by carefully tailoring the concentration of SNP suspension (Fig. 6l). The particle size in the LBIA can range from several nanometers, such as quantum dots (Fig. 6m), to even hundreds of nanometers, like polystyrene (PS) microspheres (Fig. 6o) [63,66,78,88]. Wide distribution of particle size does not affect the performance of LBIA process (see irregular commercial titaninm dioxide particles in Fig. 6n). However, narrower distribution of particle size could yield more ordered arrangement of particles (see Fig. 6o). Magnetic ferriferrous oxide NPs can also be aligned in one direction by the LBIA strategy without the assistance of externally magnetic field (Fig. 6p) [70].

2D nanomaterials

2D materials consist of a single layer of atoms, and show promising application in photovoltaics, semiconductors, electrodes and water purification due to their unusual physical characteristics. The graphene nanosheets were difficult to dissolve in the water, requiring the assistance of considerable surfactants. 1D assemblies of graphene nanosheets could be fabricated when the weight ratio of surfactant/graphene was around 15~20 (Fig. 6q) [97]. Besides arranging graphene nanosheets, the LBIA strategy can directly synthesize ordered stripes of graphdiyne (Fig. 6r) [98], a two dimensional network of benzene rings connected by diacetylenic linkages. A grooved substrate was closely integrated with a flat cooper foil, and placed in the hexaethynylbenzene-loading pyridine liquid. The liquid bridge arrays generated inside the groove gaps provided a 1D spacing for the synthesis of graphdiyne, allowing for their regular stripes that can be transferred onto a flexible polymeric substrate.

Applications of LBIA dominated 1D assemblies

LBIA strategy enables ordered patterning of 1D assemblies, indicating an effective way to precisely control the transporting route of physical signals along the 1D architecture. Towards practical applications, especially for device integration, several technical requirements are raised. For example, a large scale yet time-saving method to position metallic nanoparticles is necessary in the fabrication of electronic microcircuits. To solve this problem, a room-temperature, high-throughput and easy-to-large-scale printing technology has been proposed by Song et al. (Fig. 9a,b) [88,99–112]. Ordered GNP-loading drops were inkjet-printed onto a hydrophobic plate, serving as the microscale lyophilic domains to pin the liquid. Accordingly, microscale liquid bridges arrays could be generated to connect neighbouring printed dots. In spite of its handiness in introducing lyophilic domains onto the lyophobic substrate, the size limitation should be noticed in this strategy. Compared with the precision (several micrometers) of pillar-structured substrates fabricated by the photolithography, the size of printing dots is commonly tens of micrometers, indicating a greatly reduced density of final 1D assemblies.

Furthermore, broadening the choice of solvent species in the LBIA strategy is quite important since only soluble, or easily dispersible functional materials can be assembled. For example, functional DTT-DPP molecules (Fig. 6h) are oil soluble, rather than water soluble. In order to treat such matters, the superhydropho-

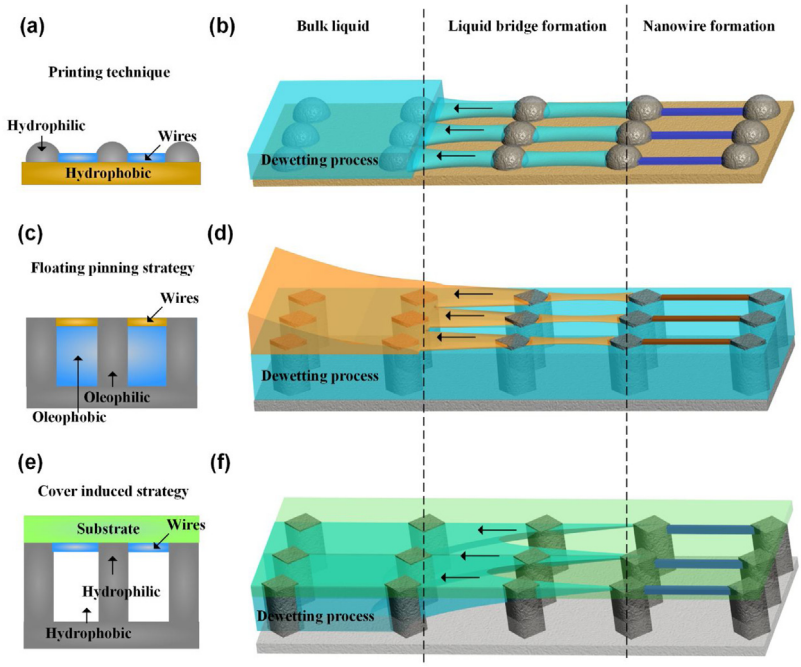

Fig. 9. Expansion of the LBIA strategy to meet different requirements of device applications. Schematical illustrations of (a,b) a printing technology to introduce lyophilic domains upon a lyophobic substrate, yielding a large scale yet time-saving method for nanoparticle patterning; (c,d) an underwater superoleophobic pillar-structured template to treat oil soluble functional materials; (e,f) a šandwichťype integration system allows for direct positioning of 1D assemblies upon the top desired substrate.

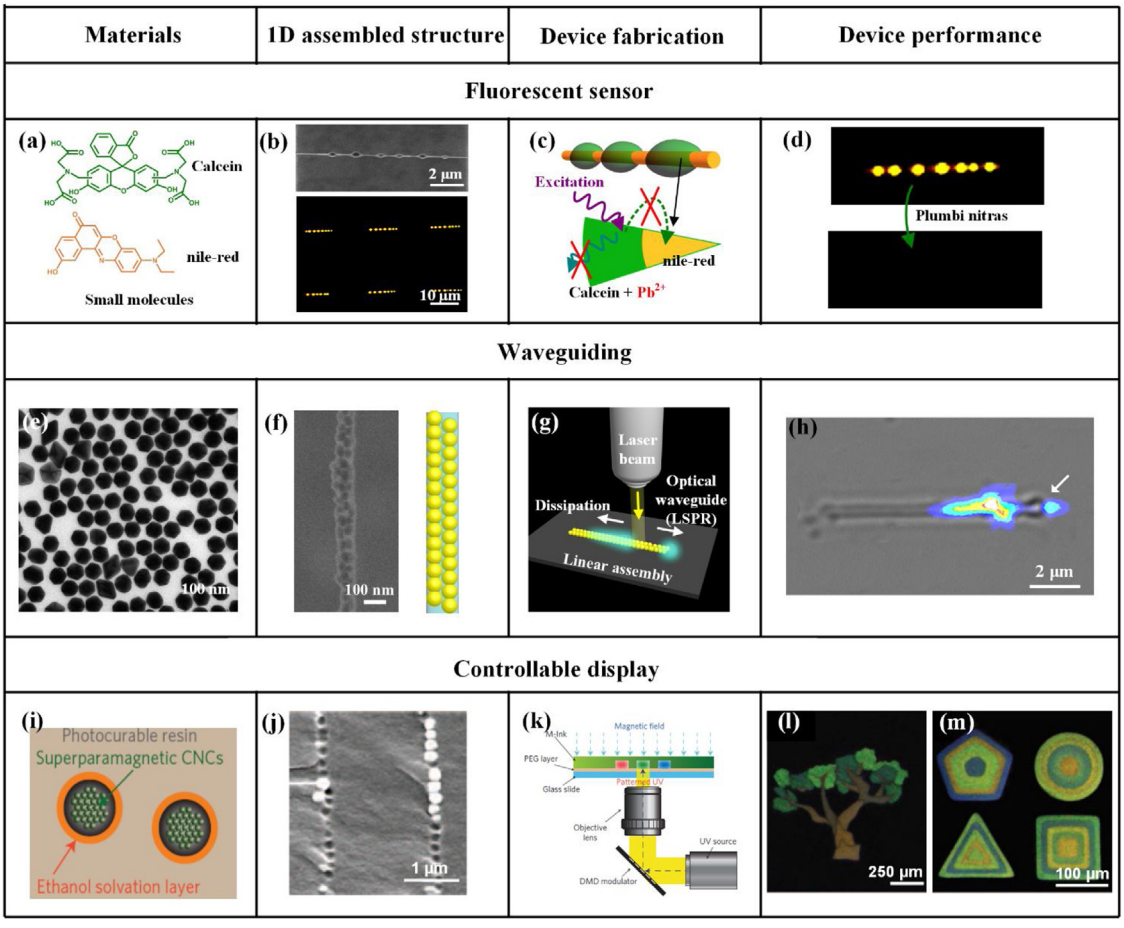

Fig. 10. Representative optical applications of LBIA resulted 1D assemblies. (a) Molecular formulas of nile-red and calcein, (e) TEM image of GNPs and (i) schematic illustration of Fe_3O_4 nanoparticles. (b), (f), (j) are 1D assemblies of (a), (e), (i) after the LBIA process, respectively. (c), (g), (k) are schematic illustrations of device integration or device testing systems. (d), (h), (l,m) are according device performances, respectively. Reprinted from Ref. [61] with permission from Royal Society of Chemistry, Ref. [67] with permission from Wiley-VCH Verlag GmbH & Co., Ref. [126] with permission from Nature Publishing Group.

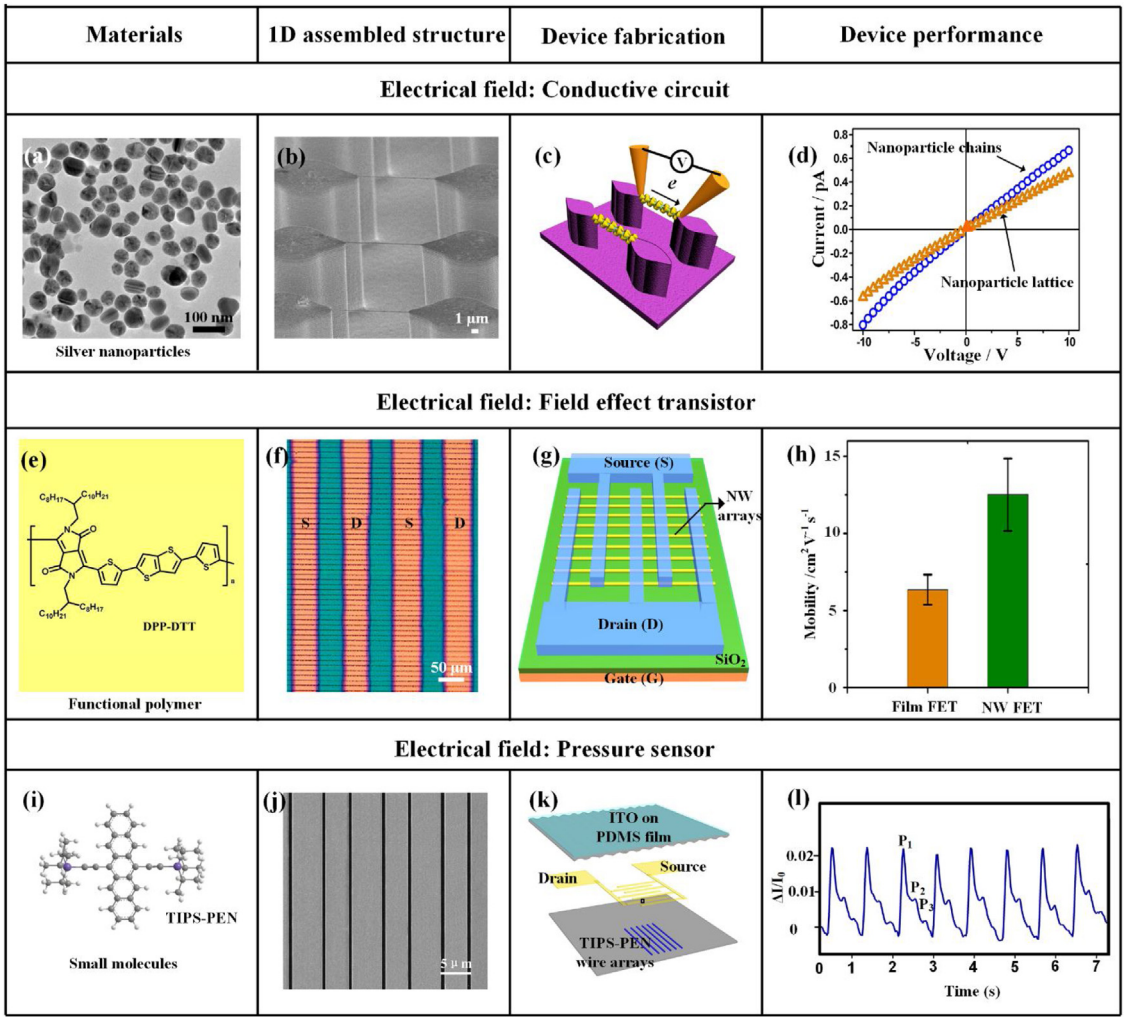

Fig. 11. Representative electrical applications of LBIA resulted 1D assemblies. (a) TEM image of SNPs, Molecular formulas of (e) DTT-DPP and (i) 6,13-bis(triisopropylsilylethynyl) pentacene (TIPS-pentacene). (b), (f), (j) are 1D assemblies of (a), (e), (i) after the LBIA process, respectively. (c), (g), (k) are schematic illustrations of device integration or device testing systems. (d), (h), (l) are according device performances, respectively. Reprinted from Ref. [58,64,65] with permission from Wiley-VCH Verlag GmbH & Co.

bic template has to be replaced by underwater superoleophobic pillar arrays (Fig. 9c,d) [64]. In most device applications, 1D assemblies of functional materials should directly grow upon the flat silicon substrates, instead of upon superhydrophobic templates. Therefore, a transfer process of as-prepared 1D assemblies from superhydrophobic templates to the desired substrates is inevitably required, indicating potential damage or loss of 1D structures. To avoid this transfer manipulation, a ‘sandwich’type integration system has been built, allowing for direct positioning of 1D assemblies upon the top desired substrates (Fig. 9e,f) [7,60,72–74]. Recently, regular lyophobic photoresist stripes [113–125] have been deposited onto a lyophilic silicon substrate to generate ordered liquid bridge arrays. The mechanism is similar to that of microgrooved method [60]. The lyophobic photoresist stripes ruptured and restricted the dewetting of liquid, allowing for the existence of numerous parallel liquid bridges at the edges of each photoresist stripes. Since the photoresists are sensitive to several organic solvents, such as acetone or chloroform, the selection of liquids, as well as related functional materials, should be carefully considered in this technology.

After inducing above-mentioned strategies to meet the device application, several representative applications of precisely patterning functional materials will be discussed, mainly focusing on the optical, electrical and magnetic fields.

Optics

Bead-shaped nile-red/calcein coaxial nanowires can be fabricated through a two-step LBIA technique (Fig. 10a). These 1D structures exhibited yellow fluorescence whereas the joint part are dark when exposed to 325 nm centered UV irradiation (Fig. 10b) [61]. Once the bead-shaped wires met the fog containing 10^{-7} wt% plumbous nitrate, their calcein beads would be directly quenched, displaying completely dark appearances (Fig. 7c,d). This local fluorescence quenching behavior shows the ability of LBIA resulted 1D assemblies to detect trace chemicals.

To break diffraction limitation of optical transport (usually more than half a wavelength of light ($\lambda/2$)), localized surface plasmon resonance (LSPR) has been recognized as an effective route to manipulate the photon transport at the nanoscale. Plasmonic waveguiding by using as-prepared GNP chains was investigated (Fig. 10e,f) [67]. A 514 nm laser beam was focused onto the NP chain, and an output light spot appeared on the right side (Fig. 10g). Owing to a great loss existing among the NPs, the propagation distance of this 1D architecture was just 2.1 μm (Fig. 10h). Even by reducing the width of NP chains down to around 100 nm, the propagation distance of SNP chains only reached up to 3.2 μm [66], which is much smaller than that required in device applications. To address this challenge, single crystalline BPEA wires were more suitable for

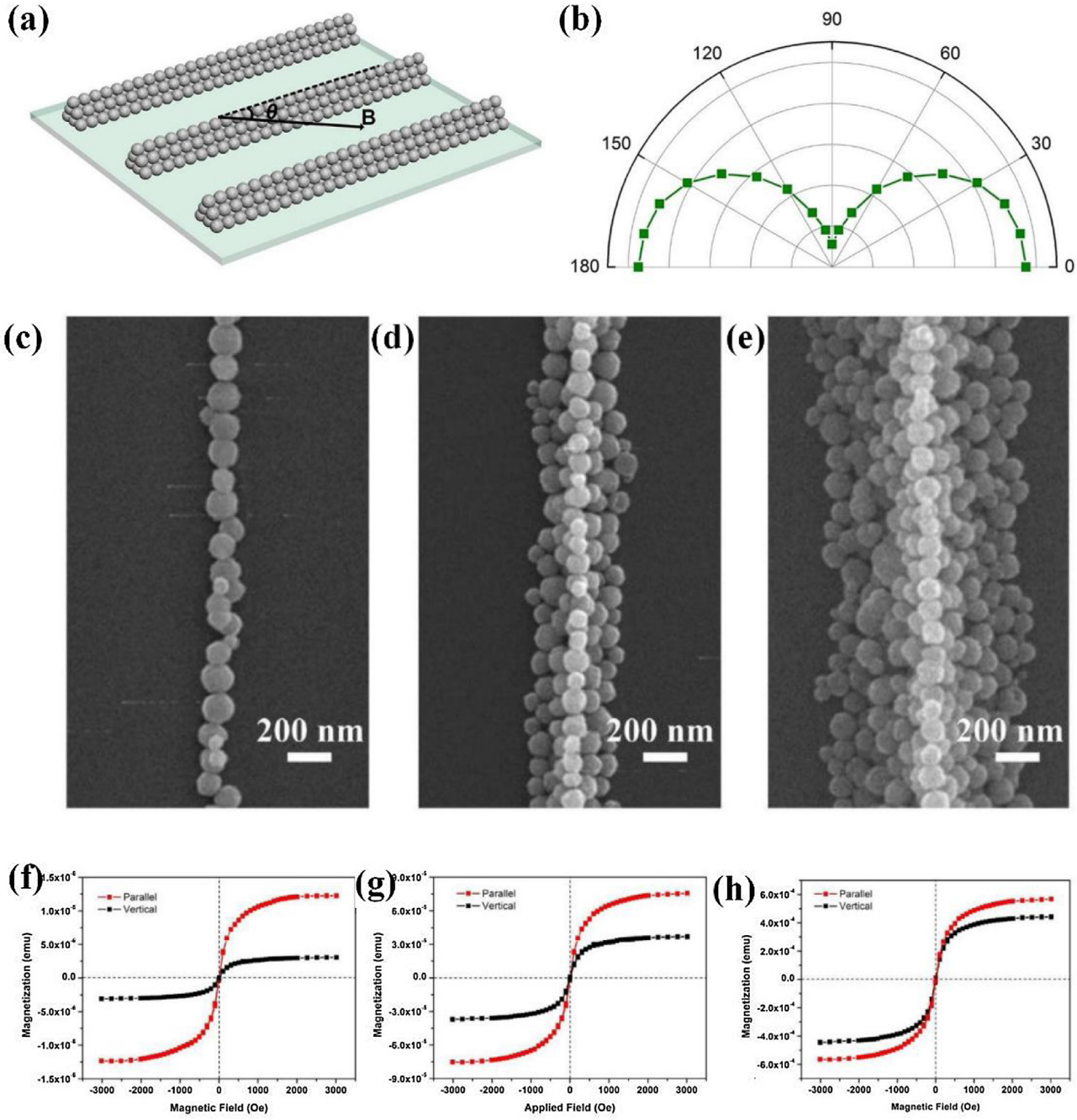

Fig. 12. Magnetic detector can be fabricated based on anisotropic property of 1D assemblies of magnetic NPs. (a) Schematic illustration of 1D assemblies of ferriferrous oxide NPs. (b) The dependence of magnetization of ferriferrous oxide NP chains on the direction of external magnetic field. Top-view SEM images of 1D assemblies of ferriferrous oxide NPs with widths of (c) 0.16, (d) 0.31, and (e) 0.82 μm, respectively. Smaller width of 1D NP assemblies indicates high aspect ratio, allowing for increased anisotropy of magnetization. (f–h) Magnetic properties of 1D assemblies of magnetic NPs in (c–e), respectively. Reprinted from Ref. [70] with permission from Wiley-VCH Verlag GmbH & Co.

waveguiding due to their regular molecular package [59,60]. The propagation distance of the light along the BPEA wire was more than 180 μm with an optical loss of 0.0131 ± 0.0004 dB μm^{-1}.

1D arrays of magnetic NPs can be used in application of color display due to their tunable 1D periodic structure and light reflectivity upon an external magnetic field. One example reported by Kwon et al. is illustrated to demonstrate the colour display application of NP 1D structures [126]. The superparamagnetic colloidal nanocrystal clusters (CNCs) were first dispersed in a mixture of ethanol and photocurable resin (Fig. 10i). In the presence of applied magnetic field, CNCs were assembled to form 1D chains, which were subsequently fixed by solidifying the resin through patterned ultraviolet exposure. The formed 1D chain structure was confirmed by SEM (Fig. 10j). The interparticle space of 1D chains could be tuned by exerting a magnetic field with different strength, resulting in desired colours. By repetitive tuning and fixing the structure colour, programmed micropatterns with different colours were successfully attained (Fig. 10k–m).

Electronics

Electrons can be guided to transport along SNP 1D assemblies. Non-conductive PDMS micropillars were used to form SNP chains (Fig. 11a,b), then tested their conductivity (Fig. 11c) [58]. Com-

pared with NP lattices, the SNP chains exhibit 1.5 times higher conductivity (Fig. 11d), which can attribute to relatively compact NP aggregations through the LBIA process. Furthermore, an oil-soluble DTT-DPP polymer has been fabricated as strictly aligned nanowire arrays by utilizing an underwater superoleophobic pillar-structured template (Fig. 11e,f) [64]. After integrating the 1D structures into a flexible field effect transistor (FET), the saturation mobility of wire devices are nearly 2 times compared with that of thin-film countpart by using the same material (Fig. 11g,h). Importantly, narrow 1D spacing of liquid bridges restricted the alignment of rigid planar macromolecules, allowing for a more regular molecular stacking compared with that prepared by traditional solution methods. These regularly packed molecules can effectively transport electrons/holes, leading to an advanced mobility in the FET applications.

Ordered packing of organic molecules can enhance the transport efficiency of electrons/holes, leading to high-performance electrical devices. In recent decade, directional shearing force in the liquids has been recognized as an effective tool to arrange the molecules. Bao's [127] and Jiang & Su's group [79] used a fluid-enhanced crystal engineering to induce the packing of TIPS-pentacene molecules (Fig. 11i,j). Owing to the directional shearing forces inside the liquid bridges, single crystalline small molecular belt arrays were fabricated, and could be integrated into a flexible pressure sensor (Fig. 11k). The as-prepared flexible device was sensitive to the external force, showing a 5.21 kPa^{-1} sensitivity during 0 and 300 Pa and a stable loading-unloading lifetime for more than 1000 cycles. Due to its excellent electrical performance, as well as the flexibility, the belt array based sensor could be attached onto the wrist of human to directly detect the pulse. Fig. 11l shows the typical pulse pressure curve consisting of three clearly different peaks (P_1 to P_3), indicating the potential of the device to monitor human health.

Magnetics

Natural creatures own a ubiquitous magnetosensitivity that help them to locate, build activities, and long-distance migration. Learning from the nature, highly oriented 1D assemblies of magnetic ferriferrous oxide NPs were fabricated though the LBIA process (Fig. 12a) [70]. Owing to linear close-packing of magnetic NPs, their magnetization intensity reached the maximum value when the magnetic field direction was parallel to their axis, whereas dropped to the minimum value in the vertical direction (Fig. 12b). The ratio of maximum/minimum magnetization intensity highly depended on the width of NP chains. By decreasing the width value from 0.82 μm to 0.16 μm, the magnetization ratio can be increased from 1.29 to 4.02 accordingly (Fig. 12c–h). This result indicates an artificial magnetic detector based on the 1D assemblies of magnetic NPs.

Conclusions

This Review summarizes recent progress on precisely positioning 1D patterning, from small molecules to macromolecules and nanomaterials, through a LBIA strategy. The mechanism, rules for selecting the functional materials and strategies to tune the locations and structures of 1D assembles are discussed in detail. Owing to anisotropic linear structure, tunable material species, controllable molecular packing, and on-demand positioning upon a desired substrate, the 1D assemblies dominated by the LBIA process can find promising application in optical, electrical and magnetic fields.

The research on LBIA strategy has just started, and considerable challenges exist in its development. First, most functional materials dissolve in organic solvents, rather than water. To control the dewetting process of organic solvents with different surface tensions ranging from ~20 to ~60 dyn/cm, the lyophilic/lyophobic domains or substrates should be carefully designed according to the organic liquids. Secondly, assembling small molecules into single crystalline 1D microstructures can facilitate the waveguiding, [59,60], highly sensitive photodetectior [128] or even the laser field [72–74]. Careful selection of functional molecular segments and related organic solvent to favor the close-packing of small molecules will be the key in this direction. Thirdly, the transport loss of NP based 1D structures is considerable, especially in optical application [66,67]. Alternatively, the application of these NP chains to detect the field [70] or gas sensors [129] are promising. The key advantage of LBIA strategy is the employment of self-contractive liquid bridges as confined spacing to restrict 1D assembly of guest materials. Accordingly, this soft confined spacing can be narrower down to several nanometer size, leading to NP chains with single NP in width (Fig. 6l). This feature can also facilitate the nonlinear polymer rheology and DNA technology in future [94,95]. Finally, we believe that ordered 1D assemblies/structures of functional materials through the LBIA process will offer new opportunities that might favor different application fields.

Acknowledgements

This work was supported by National 1000 Young Talents Program of China, and initiatory financial support from Huazhong University of Science and Technology (HUST).

References

[1] J. Xiang, W. Lu, Y.J. Hu, Y. Wu, H. Yan, C.M. Lieber, Nature 441 (2006) 489–493.
[2] Y. Huang, X.F. Duan, Y. Cui, L.J. Lauhon, K.H. Kim, C.M. Lieber, Science 294 (2001) 1313–1317.
[3] J.W. Liu, H.W. Liang, S.H. Yu, Chem. Rev. 112 (2012) 4770–4799.
[4] P. Song, H.L. Qin, H.L. Gao, H.P. Cong, S.H. Yu, Nat. Commun. 9 (2018) 2786.
[5] B.G. Chen, H. Wu, C.G. Xin, D.X. Dai, L.M. Tong, Nat. Commun. 8 (2017) 20.
[6] S. Gazibegovic, D. Car, H. Zhang, S.C. Balk, J.A. Logan, M.W.A. de Moor, M.C. Cassidy, R. Schmits, D. Xu, G.Z. Wang, P. Krogstrup, R.L.M.O.H. Veld, K. Zuo, Y. Vos, J. Shen, D. Bouman, B.S. Hojaei, D. Pennachio, J.S. Lee, P.J. van Veldhoven, S. Koelling, M.A. Verheijen, L.P. Kouwenhoven, C.J. Palmstrom, E.P.A.M. Bakkers, Nature 548 (2017) 434–438.
[7] H.F. Gao, J.G. Feng, B. Zhang, C.Y. Xiao, Y.C. Wu, X.N. Kan, B. Su, Z.H. Wang, W.P. Hu, Y.M. Sun, L. Jiang, A.J. Heeger, Adv. Funct. Mater. 27 (2017), 1701347.
[8] J. Chen, P. Yu, J. Stenger, M. Hocevar, D. Car, S.R. Plissard, E.P.A.M. Bakkers, T.D. Stanescu, S.M. Frolov, Sci. Adv. 3 (2017), 1701476.
[9] J. Kim, H.C. Lee, K.H. Kim, M.S. Hwang, J.S. Park, J.M. Lee, J.P. So, J.H. Choi, S.H. Kwon, C.J. Barrelet, H.G. Park, Nat. Nanotechnol. 12 (2017) 963–968.
[10] H.M. Fahad, H. Shiraki, M. Amani, C.C. Zhang, V.S. Hebbar, W. Gao, H. Ota, M. Hettick, D. Kiriya, Y.Z. Chen, Y.L. Chueh, A. Javey, Sci. Adv. 3 (2017), 1602557.
[11] C.C. Chiang, C.Y. Hung, S.W. Chou, J.J. Shyue, K.Y. Cheng, P.J. Chang, Y.Y. Yang, C.Y. Lin, T.K. Chang, Y. Chi, H.L. Chou, P.T. Chou, Adv. Funct. Mater. 28 (2018), 1870020.
[12] S.H. Gong, F. Alpeggiani, B. Sciacca, E.C. Garnett, L. Kuipers, Science 359 (2018) 443–447.
[13] C.Y. Hwang, W.J. Song, J.G. Han, S. Bae, G. Song, N.S. Choi, S. Park, H.K. Song, Adv. Mater. 30 (2018), 1705445.
[14] O. Gul, H. Zhang, J.D.S. Bommer, M.W.A. de Moor, D. Car, S.R. Plissard, E.P.A.M. Bakkers, A. Geresdi, K. Watanabe, T. Taniguchi, L.P. Kouwenhoven, Nat. Nanotechnol. 13 (2018) 192–197.
[15] A. Curtis, C. Calvi, J. Tinsley, R. Hollinger, V. Kaymak, A. Pukhov, S.J. Wang, A. Rockwood, Y. Wang, V.N. Shlyaptsev, J.J. Rocca, Nat. Commun. 9 (2018), 1077.
[16] R.X. Bian, Y. Jiang, Y. Wang, J.K. Sun, J.S. Hu, L. Jiang, H. Liu, Adv. Funct. Mater. 28 (2018), 1707408.
[17] S.Y. Chen, Y.L. Tang, K. Zhan, D.H. Sun, X. Hou, Nano Today 20 (2018) 84–100.
[18] A. Anand, C.H. Chi, S. Banerjee, M.Y. Chou, F.G. Tseng, C.Y. Pan, Y.T. Chen, Small 14 (2018), 1704439.
[19] T.H. Kim, S.W. Kang, J.W. Heo, S.S. Cho, J.W. Kim, A. Choe, B. Walker, R. Shanker, H.H. Ko, J.Y. Kim, Adv. Mater. 30 (2018), 1800659.
[20] L. Gao, L. Chen, H. Wei, H.X. Xu, Nanoscale 10 (2018), 14771-14771.
[21] S. Kang, S. Cho, R. Shanker, H. Lee, J. Park, D.S. Um, Y. Lee, H. Ko, Sci. Adv. 4 (2018), 8772.
[22] Y. Yang, J.L. Wang, L. Liu, Z.H. Wang, J.W. Liu, S.H. Yu, Nanoscale 9 (2017) 52–55.

[23] N.P. Dasgupta, J.W. Sun, C. Liu, S. Brittman, S.C. Andrews, J. Lim, H.W. Gao, R.X. Yan, P.D. Yang, Adv. Mater. 26 (2014) 2137–2184.
[24] R. Requist, P.P. Baruselli, A. Smogunov, M. Fabrizio, S. Modesti, E. Tosatti, Nat. Nanotechnol. 11 (2016) 499–508.
[25] R. Beckman, E. Johnston-Halperin, Y. Luo, J.E. Green, J.R. Heath, Science 310 (2005) 465–468.
[26] X.P. Chen, C.K.Y. Wong, C.A. Yuan, G.Q. Zhang, Sens. Actuator B-Chem. 177 (2013) 178–195.
[27] S.M. Yoo, M. Kang, T. Kang, D.M. Kim, S.Y. Lee, B. Kim, Nano Lett. 13 (2013) 2431–2435.
[28] H. Yan, J.N. Hohman, F.H. Li, C.J. Jia, D. Solis-Ibarra, B. Wu, J.E.P. Dahl, R.M.K. Carlson, B.A. Tkachenko, A.A. Fokin, P.R. Schreiner, A. Vailionis, T.R. Kim, T.P. Devereaux, Z.X. Shen, N.A. Melosh, Nat. Mater. 16 (2017) 349–355.
[29] L. Xu, Y.L. Zhao, K.A. Owusu, Z.C. Zhuang, Q. Liu, Z.Y. Wang, Z.H. Li, L.Q. Mai, Chem-US 4 (2018) 1538–1559.
[30] T. Lei, J. Pei, J. Mater. Chem. 22 (2012) 785–798.
[31] N. Rossi, F.R. Braakman, D. Cadeddu, D. Vasyukov, G. Tutuncuoglu, A.F.I. Morral, M. Poggio, Nat. Nanotechnol. 12 (2017) 150–155.
[32] H. Zhang, O. Gul, S. Conesa-Boj, M.P. Nowak, M. Wimmer, K. Zuo, V. Mourik, F.K. de Vries, J. van Veen, M.W.A. de Moor, J.D.S. Bommer, D.J. van Woerkom, D. Car, S.R. Plissard, E.P.A.M. Bakkers, M. Quintero-Perez, M.C. Cassidy, S. Koelling, S. Goswami, K. Watanabe, T. Taniguchi, L.P. Kouwenhoven, Nat. Commun. 8 (2017), 16025.
[33] X.Y. Li, P.J. Wolanin, L.R. MacFarlane, R.L. Harniman, J.S. Qian, O.E.C. Gould, T.G. Dane, J. Rudin, M.J. Cryan, T. Schmaltz, H. Frauenrath, M.A. Winnik, C.F.J. Faul, I. Manners, Nat. Commun. 8 (2017), 15909.
[34] C.H. Zhang, C.L. Zou, H.Y. Dong, Y.L. Yan, J.N. Yao, Y.S. Zhao, Sci. Adv. 3 (2017), 1700225.
[35] C. Lu, S. Park, T.J. Richner, A. Derry, I. Brown, C. Hou, S.Y. Rao, J. Kang, C.T. Moritz, Y. Fink, P. Anikeeva, Sci. Adv. 3 (2017), 1600955.
[36] L.Q. Zhang, Y.S. Tang, Q.M. Peng, T.T. Yang, Q.N. Liu, Y.C. Wang, Y.F. Li, C.C. Du, Y. Sun, L.S. Cui, F. Yang, T.D. Shen, Z.W. Shan, J.Y. Huang, Nat. Commun. 9 (2018), 96.
[37] L. Xu, H.W. Liang, Y. Yang, S.H. Yu, Chem. Rev. 118 (2018) 3209–3250.
[38] H. Ali, Y.Y. Zhang, J. Tang, K. Peng, S.B. Sun, Y. Sun, F.L. Song, A. Falak, S.Y. Wu, C.J. Qian, M. Wang, Z.C. Zuo, K.J. Jin, A.M. Sanchez, H.Y. Liu, X.L. Xu, Small 14 (2018), 1704429.
[39] I. Madan, J. Buh, V.V. Baranov, V.V. Kabanov, A. Mrzel, D. Mihailovic, Sci. Adv. 4 (2018) 0043.
[40] Y.B. Luo, X. Yan, J.N. Zhang, B. Li, Y. Wu, Q.C. Lu, C.X.S. Jin, X. Zhang, X.M. Ren, Nanoscale 10 (2018) 9212–9217.
[41] B.W. An, S. Heo, S. Ji, F. Bien, J.U. Park, Nat. Commun. 9 (2018), 2458.
[42] D. Zhu, Q.Y. Zhao, H. Choi, T.J. Lu, A.E. Dane, D. Englund, K.K. Berggren, Nat. Nanotechnol. 13 (2018) 596–601.
[43] C.S. Shang, Y.X. Guo, E.K. Wang, Nano Res. 11 (2018) 4348–4355.
[44] A. Senichev, P. Corfdir, O. Brandt, M. Ramsteiner, S. Breuer, J. Schilling, L. Geelhaar, P. Werner, Nano Res. 11 (2018) 4708–4721.
[45] S.Z. Oener, A. Cavalli, H.Y. Sun, J.E.M. Haverkort, E.P.A.M. Bakkers, E.C. Garnett, Nat. Commun. 9 (2018), 3248.
[46] Y.X. Zhou, R.K. Chen, J.Y. Wang, Y.S. Huang, M. Li, Y.J. Xing, J.H. Duan, J.J. Chen, J.D. Farrell, H.Q. Xu, J.N. Chen, Adv. Mater. 30 (2018), 1802551.
[47] H. Yang, V. Khayrudinov, V. Dhaka, H. Jiang, A. Autere, H. Lipsanen, Z.P. Sun, H. Jussila, Sci. Adv. 4 (2018) 7954.
[48] Y.Y. Wang, M.M. Zhao, Q.X. Zhao, Q. Li, H. Pang, Nanoscale 10 (2018) 15755–15762.
[49] J. Moon, U. Sim, D.J. Kim, H.Y. Ahn, J. An, H. Ha, K.S. Choi, C. Jeon, J. Lee, K.T. Nam, B.H. Hong, Nanoscale 10 (2018) 13936–13941.
[50] B. Su, L. Jiang, X.C. Jiang, A.B. Yu, Powder Technol. 312 (2017) 103–112.
[51] B. Su, Y. Tian, L. Jiang, J. Am. Chem. Soc. 138 (2016) 1727–1748.
[52] M.K. Chaudhury, G.M. Whitesides, Science 256 (1992) 1539–1541.
[53] S. Daniel, M.K. Chaudhury, J.C. Chen, Science 291 (2001) 633–636.
[54] J.A. Lv, Y.Y. Liu, J. Wei, E.Q. Chen, L. Qin, Y.L. Yu, Nature 537 (2016) 179–184.
[55] B. Su, S.T. Wang, J. Ma, Y.C. Wu, X. Chen, Y.L. Song, L. Jiang, Adv. Mater. 24 (2012) 559–564.
[56] C. Zou, J.X. Wang, M. Wang, Y.C. Wu, K.H. Gu, Z.H. Shen, G.R. Xiong, H. Yang, L. Jiang, T. Ikeda, Small 14 (2018), 1800557.
[57] Y. Liu, J.G. Feng, B. Zhang, Y.C. Wu, Y. Chen, L. Jiang, Small 14 (2018), 1701861.
[58] X.Y. Jiang, Y.C. Wu, B. Su, R.G. Xie, W.S. Yang, L. Jiang, Small 10 (2014) 258–264.
[59] J.G. Feng, Y.C. Wu, B. Su, L. Jiang, Small 11 (2015) 5759–5765.
[60] Y.C. Wu, J.G. Feng, X.Y. Jiang, Z. Zhang, X.D. Wang, B. Su, L. Jiang, Nat. Commun. 6 (2015), 6737.
[61] Y. Wu, B. Bao, B. Su, L. Jiang, J. Mater. Chem. A 1 (2013) 8581–8586.
[62] B. Su, Y.C. Wu, L. Jiang, Chem. Soc. Rev. 41 (2012) 7832–7856.
[63] B. Zhang, F.S. Meng, J.G. Feng, J.X. Wang, Y.C. Wu, L. Jiang, Adv. Mater. 30 (2018), 1707291.
[64] Y.C. Wu, B. Su, L. Jiang, A.J. Heeger, Adv. Mater. 25 (2013) 6526–6533.
[65] Y.C. Wu, J.G. Feng, B. Su, L. Jiang, Adv. Mater. 28 (2016) 2266–2273.
[66] B. Su, C. Zhang, S.R. Chen, X.Y. Zhang, L.F. Chen, Y.C. Wu, Y.W. Nie, X.N. Kan, Y.L. Song, L. Jiang, Adv. Mater. 26 (2014) 2501–2507.
[67] B. Su, Y.C. Wu, Y. Tang, Y. Chen, W.L. Cheng, L. Jiang, Adv. Mater. 25 (2013) 3968–3972.
[68] B. Su, S.T. Wang, Y.C. Wu, X. Chen, Y.L. Song, L. Jiang, Adv. Mater. 24 (2012) 2780–2785.
[69] Y. Liu, W. Hao, H.Y. Yao, S.Z. Li, Y.C. Wu, J. Zhu, L. Jiang, Adv. Mater. 30 (2018), 1705377.
[70] X.Y. Jiang, J.G. Feng, L. Huang, Y.C. Wu, B. Su, W.S. Yang, L.Q. Mai, L. Jiang, Adv. Mater. 28 (2016) 6952–6958.
[71] J.G. Feng, X.X. Yan, Y.F. Zhang, X.D. Wang, Y.C. Wu, B. Su, H.B. Fu, L. Jiang, Adv. Mater. 28 (2016) 3732–3741.
[72] J.G. Feng, X.X. Yan, Y. Liu, H.F. Gao, Y.C. Wu, B. Su, L. Jiang, Adv. Mater. 29 (2017), 1605993.
[73] J.G. Feng, Q. Song, B. Zhang, Y.C. Wu, T. Wang, L. Jiang, Adv. Mater. 29 (2017), 1703143.
[74] J.G. Feng, X.Y. Jiang, X.X. Yan, Y.C. Wu, B. Su, H.B. Fu, J.N. Yao, L. Jiang, Adv. Mater. 29 (2017), 1603652.
[75] Y.C. Wu, X. Chen, B. Su, Y.L. Song, L. Jiang, Adv. Funct. Mater. 22 (2012) 4569–4576.
[76] X.N. Kan, C.Y. Xiao, H.F. Gao, Z.H. Wang, Y.C. Wu, B. Su, J.Q. Zhang, Z.X. Wei, B. Kong, W.P. Hu, Y.M. Sun, L. Jiang, A.J. Heeger, Adv. Electron. Mater. 2 (2016), 1600111.
[77] Y.C. Wu, S. Su, L. Jiang, ACS Nano 6 (2012) 9005–9012.
[78] Y.Z. Wang, C. Wei, H.L. Cong, Q. Yang, Y.C. Wu, B. Su, Y.S. Zhao, J.X. Wang, L. Jiang, ACS Appl. Mater. Interface 8 (2016) 4985–4993.
[79] X.N. Kan, C.Y. Xiao, X.M. Li, B. Su, Y.C. Wu, W. Jiang, Z.H. Wang, L. Jiang, ACS Appl. Mater. Interface 8 (2016) 18978–18984.
[80] J.J. Guan, N. Ferrell, B. Yu, D.J. Hansford, L.J. Lee, Soft Matter 3 (2007) 1369–1371.
[81] J.J. Guan, J. Lee, Proc. Natl. Acad. Sci. U. S. A. 102 (2005) 18321–18325.
[82] P.E. Boukany, A. Morss, W.C. Liao, B. Henslee, H.C. Jung, X.L. Zhang, B. Yu, X.M. Wang, Y. Wu, L. Li, K.L. Gao, X. Hu, X. Zhao, O. Hemminger, W. Lu, G.P. Lafyatis, L.J. Lee, Nat. Nanotechnol. 6 (2011) 747–754.
[83] S.N. Wang, J.J. Guan, L.J. Lee, ChemPhysChem 9 (2008) 967–973.
[84] C.H. Lin, J.J. Guan, S.W. Chau, S.C. Chen, L.J. Lee, Biomicrofluidics 4 (2010), 034103.
[85] J.J. Guan, B. Yu, L.J. Lee, Adv. Mater. 19 (2007) 1212–1217.
[86] J.J. Guan, P.E. Boukany, O. Hemminger, N.R. Chiou, W.B. Zha, M. Cavanaugh, L.J. Lee, Adv. Mater. 22 (2010) 3997–4001.
[87] P.J. Glazer, L. Bergen, L. Jennings, A.J. Houtepen, E. Mendes, P.E. Boukany, Small 10 (2014) 1729–1734.
[88] D. Guo, Y.N. Li, X. Zheng, F.Y. Li, S.R. Chen, M.Z. Li, Q. Yang, H.Z. Li, Y.L. Song, J. Am. Chem. Soc. 140 (2018) 18–21.
[89] P.J. Glazer, Q. Warringa, L. Bergen, P.E. Boukany, IEEE Eng. Med. Biol. (2015) 2187–2190.
[90] E. Miele, A. Accardo, A. Falqui, M. Marini, A. Giugni, M. Leoncini, F. De Angelis, R. Krahne, E. Di Fabrizio, Small 11 (2015) 134–140.
[91] G. Ciasca, L. Businaro, M. Papi, A. Notargiacomo, M. Chiarpotto, A. De Ninno, V. Palmieri, S. Carta, E. Giovine, A. Gerardino, M. De Spirito, Nanotechnology 24 (2013) 495302–495308.
[92] G. Ciasca, M. Papi, M. Chiarpotto, A. De Ninno, E. Giovine, G. Campi, A. Gerardino, M. De Spirito, L. Businaro, Nano-Micro Lett. 6 (2014) 280–286.
[93] G. Ciasca, M. Papi, V. Palmieri, M. Chiarpotto, S. Di Claudio, A. De Ninno, E. Giovine, G. Campi, A. Gerardino, L. Businaro, M. De Spirito, Nano-Micro Lett. 7 (2015) 146–151.
[94] W.C. Liao, X. Hu, W.X. Wang, L.J. Lee, Biomicrofluidics 7 (2013), 034103.
[95] L. Rems, D. Kawale, L.J. Lee, P.E. Boukany, Biomicrofludics 10 (2016), 043403.
[96] E. Miele, S. Raj, Z. Baraissov, P. Kral, U. Mirsaidov, Adv. Mater. 29 (2017), 1702682.
[97] X.N. Kan, B. Su, L. Jiang, Small 10 (2014) 2570–2577.
[98] S.S. Wang, H.B. Liu, X.N. Kan, L. Wang, Y.H. Chen, B. Su, Y.L. Li, L. Jiang, Small 13 (2017), 1602265.
[99] S.R. Chen, M. Su, C. Zhang, M. Gao, B. Bao, Q. Yang, B. Su, Y.L. Song, Adv. Mater. 27 (2015) 3928–3935.
[100] B. Bao, J.K. Jiang, F.Y. Li, P.C. Zhang, S.R. Chen, Q. Yang, S.T. Wang, B. Su, L. Jiang, Y.L. Song, Adv. Funct. Mater. 25 (2015) 3286–3294.
[101] J.K. Jiang, B. Bao, M.Z. Li, J.Z. Sun, C. Zhang, Y. Li, F.Y. Li, X. Yao, Y.L. Song, Adv. Mater. 28 (2016) 1420–1426.
[102] M. Su, F.Y. Li, S.R. Chen, Z.D. Huang, M. Qin, W.B. Li, X.Y. Zhang, Y.L. Song, Adv. Mater. 28 (2016) 1369–1374.
[103] D. Guo, C. Li, Y. Wang, Y.N. Li, Y.L. Song, Angew. Chem. Int. Ed. 56 (2017) 15348–15352.
[104] Y. Huang, W.B. Li, M. Qin, H.H. Zhou, X.Y. Zhang, F.Y. Li, Y.L. Song, Small 13 (2017), 1503339.
[105] Z.D. Huang, M. Su, Q. Yang, Z. Li, S.R. Chen, Y.F. Li, X. Zhou, F.Y. Li, Y.L. Song, Nat. Commun. 8 (2017) 14110.
[106] M. Su, Z.D. Huang, Y. Huang, S.R. Chen, X. Qian, W.B. Li, Y.F. Li, W.H. Pei, H.D. Chen, F.Y. Li, Y.L. Song, Adv. Mater. 29 (2017), 1605223.
[107] M. Gao, M.X. Kuang, L.H. Li, M.J. Liu, L.B. Wang, Y.L. Song, Small 14 (2018), 1800117.
[108] Y.F. Li, M. Su, Z. Li, Z.D. Huang, F.Y. Li, Q. Pan, W.J. Ren, X.T. Hu, Y.L. Song, Small 14 (2018), 1800792.
[109] M. Su, Z.D. Huang, Y.F. Li, X. Qian, Z. Li, X.T. Hu, Q. Pan, F.Y. Li, L.H. Li, Y.L. Song, Adv. Mater. 30 (2018), 1870014.
[110] Z.D. Huang, M. Su, Q. Yang, Z. Li, S.R. Chen, Y.F. Li, X. Zhou, F.Y. Li, Y.L. Song, Nat. Commun. 8 (2017) 14110.
[111] Z.K. Gu, Z.D. Huang, C. Li, M.Z. Li, Y.L. Song, Sci. Adv. 4 (2018), 2390.
[112] D. Guo, Y.L. Song, Chem.-Eur. J. 24 (2018) 16196–16208.
[113] C.Y. Zhang, X.J. Zhang, X.H. Zhang, X. Fan, J.S. Jie, J.C. Chang, C.S. Lee, W.J. Zhang, S.T. Lee, Adv. Mater. 20 (2008) 1716–1723.

[114] R.R. Bao, C.Y. Zhang, Z.L. Wang, X.J. Zhang, X.M. Ou, C.S. Lee, J.S. Jie, X.H. Zhang, Chem.-Eur. J. 18 (2012) 975–980.
[115] Y.M. Wu, X.J. Zhang, H.H. Pan, W. Deng, X.H. Zhang, X.W. Zhang, J.S. Jie, Sci. Rep.-U. K. 3 (2013) 1–8.
[116] C. Gong, W. Deng, B. Zou, Y.L. Xing, X.J. Zhang, X.H. Zhang, J.S. Jie, ACS Appl. Mater. Interface 6 (2014) 11018–11024.
[117] W. Deng, X.J. Zhang, L. Wang, J.C. Wang, Q.X. Shang, X.H. Zhang, L.M. Huang, J.S. Jie, Adv. Mater. 27 (2015) 7305–7321.
[118] X.J. Zhang, J.S. Jie, W. Deng, Q.X. Shang, J.C. Wang, H. Wang, X.F. Chen, X.H. Zhang, Adv. Mater. 28 (2016) 2475–2503.
[119] W. Deng, X.J. Zhang, X.H. Zhang, J.H. Guo, J.S. Jie, Adv. Mater. Technol.-U. S. 2 (2017), 1600280.
[120] W. Wang, L. Wang, G.L. Dai, W. Deng, X.J. Zhang, J.S. Jie, X.H. Zhang, Nano-Micro Lett. 9 (2017), 52.
[121] Y.D. Zhang, J.S. Jie, Y.N. Sun, S.G. Jeon, X.J. Zhang, G.L. Dai, C.J. Lee, X.H. Zhang, Small 13 (2017), 1604261.
[122] L. Wang, X.J. Zhang, G.L. Dai, W. Deng, J.S. Jie, X.H. Zhang, Nano Res. 11 (2018) 882–891.
[123] X.Z. Xu, X.J. Zhang, W. Deng, L.M. Huang, W. Wang, J.S. Jie, X.H. Zhang, ACS Appl. Mater. Interface 10 (2018) 10287–10295.
[124] X.Z. Xu, X.J. Zhang, W. Deng, J.S. Jie, X.H. Zhang, Small Methods 2 (2018), 1700340.
[125] X.J. Zhang, J. Mao, W. Deng, X.Z. Xu, L.M. Huang, X.H. Zhang, S.T. Lee, J.S. Jie, Adv. Mater. 30 (2018), 1800187.
[126] H. Kim, J.P. Ge, J. Kim, S. Choi, H. Lee, H. Lee, W. Park, Y. Yin, S. Kwon, Nat. Photonics 3 (2009) 534–540.
[127] Y. Diao, B.C.K. Tee, G. Giri, J. Xu, D.H. Kim, H.A. Becerril, R.M. Stoltenberg, T.H. Lee, G. Xue, S.C.B. Mannsfeld, Z.N. Bao, Nat. Mater. 12 (2013) 665–671.
[128] J.G. Feng, C. Gong, H.F. Gao, W. Wen, Y.J. Gong, X.Y. Jiang, B. Zhang, Y.C. Wu, Y.S. Wu, H.B. Fu, L. Jiang, X. Zhang, Nat. Electron 1 (2018) 404–410.
[129] Y. Tang, B. Su, M.S. Liu, Y. Feng, X.C. Jiang, L. Jiang, A.B. Yu, Small 13 (2017), 1601087.

Chunze Yan is currently a full professor at the Huazhong University of Science and Technology (HUST) and deputy director of the State Key Laboratory of Material Processing and Die & Mould Technology. He received his B.S. degree in applied chemistry (2000) and Ph.D. degree in materials processing engineering (2009) from HUST. He then worked as a postdoctoral research fellow at the University of Exeter in UK from 2010 to 2015. In 2016, he was awarded the Hundred Talents Program in Hubei Province and joined HUST as an associate professor. Then, he was exceptionally promoted to a full professor in 2017. His research works have engaged in material preparation and additive manufacturing (AM), and especially focused on micro/nano composites and their powder bed fusion AM processes.

Bin Su is currently a full professor in the School of Materials Science and Engineering, Huazhong University of Science and Technology (HUST). He obtained his B.S. degree (2005), and Ph.D. degree (2009) from Shanghai Jiao Tong University. Then, he worked as a postdoctoral fellow (2010), assist professor (2011) and associate professor (2012) in Prof. Lei Jiang's group at ICCAS. In 2014, he worked at Monash University as an ARC-DECRA research fellow, then joined HUST in 2018. His research interest focuses on LBIA dominated patternings and exploiting their applications as flexible optical/electrical devices.

Yusheng Shiis currently acting as the Huazhong Scholar leading Special Term Professor in Huazhong University of Science and Technology (HUST), and undertaking several duties including the secretary of the CCP committee of School of Materials Science and Engineering in HUST, director of national-local united engineering laboratory (Hubei) of numerical materials processing technology and equipment, chief scientist of theme expert group in innovation special zone of national defense science and technology, committee member of expert board in industrial alliance of Chinese additive manufacturing, vice-director committee member of additive manufacturing branch of Chinese Mechanical Engineering Society, vice-chairman of world 3D printing alliance, and chairman of Hubei provincial 3D printing alliance. His research interest focuses on additive manufacturing and related material applications.

Lei Jiang is a full professor at TIPCCAS. He obtained his B.S. degree (1987), M.S. degree (1990), and Ph.D. degree (1994) from Jilin University (Tiejin Li's group). He then worked as a postdoctoral fellow in Prof. Akira Fujishima's group at Tokyo University, and as a senior researcher at Kanagawa Academy of Sciences and Technology under Prof. Kazuhito Hashimoto. In 1999, he joined the ICCAS as the Hundred Talents program and moved to TIPCCAS in 2015. He was elected as members of the Chinese Academy of Sciences (2009), the World Academy of Sciences (2012) and as a foreign member of the US National Academy of Engineering (2016). His research interest focuses on bioinspired smart interfacial materials.